Rev.Adv.Mater.Sci. 15(2007) 179-184

THE STRUCTURAL AND ELECTRON FIELD EMISSION PROPERTIES OF ION- BEAM-SYNTHESISED METALLIC-DIELECTRIC NANOCOMPOSITES

W.M. Tsang[1], V. Stolojan[1], S.P. Wong[2], J.K.N. Linder[3], B.J. Sealy[1] and S.R.P. Silva[1]

[1]Nanoelectronics Centre, Advanced Technology Institute, School of Electronics and Physical Sciences, University of Surrey, Guildford, GU2 7XH, United Kingdom
[2]Department of Electronic Engineering, Chinese University of Hong Kong, Hong Kong
[3]Universität Augsburg, Institut für Physik, D-86135 Augsburg, Germany

Received: January 22, 2007

Abstract. Metallic-dielectric nanocomposites, including Ag-SiO_2, Co-SiO_2, and WC-SiC, were synthesised on silicon substrates using ion implantation. The electron field emission (FE) properties of these nanocomposites were studied and correlated to their microstructure using atomic force microscopy, Rutherford backscattering spectroscopy, X-ray photoelectron spectroscopy and transmission electron microscopy. These nanocomposite layers exhibit excellent FE properties and give an emission current of 1 nA at the applied electric fields of as low as 5 V/μm for Co-SiO_2 nanocomposites. Moreover, the results clearly show that isolated metallic nanoclusters embedded in a relatively electrically insulating matrix, can create local field enhancement for the samples, which we attribute to the enhancement factor associated with electrical inhomogeneity effects.

1. INTRODUCTION

Metallic nanoclusters embedded in dielectric matrices (i.e. metallic-dielectric nanocomposites) have attracted a significant research interest from the community over several decades because of their unique optical and magnetic properties. For instance, metal nanoclusters embedded in a glass matrix exhibit an enhanced optical Kerr susceptibility and picosecond response time, thus make them of interesting to the optoelectronic device community [1,2]. Furthermore, isolated ferromagnetic nanoparticles embedded in the dielectric are promising candidates for the next generation ultra-high-density magnetic data storage [3,4]. In this work, we demonstrate that metallic-dielectric nanocomposite layers have excellent field emission (FE) properties. Electrons can be easily extracted out from their surface to vacuum, by the electron FE process under relatively low electric fields (≤20 V/μm), when compared with several thousand volts per micrometer for flat metallic cathodes. This phenomenon originates from the local field enhancement associated with the electrical inhomogeneity between the metallic nanoclusters and the host matrix [5-8]. Hence, they can potentially form the basis for the next generation vacuum nanoelectronic electron sources.

In this work, metallic-dielectric nanocomposites were synthesised on silicon (Si) substrates using ion implantation. In comparison to other fabrication techniques, such as sol-gel synthesis and sputtering, ion implantation has attracted significant interest due to the possibility of; patterning the materials, overcoming the doping solubility limits and being able to introduce virtually any metallic

Corresponding author: W.M. Tsang, e-mail: wmtsang@alumni.cuhk.net

element into any dielectric matrix, in accurate quantities at fixed depths. At first, either thermally oxidised silicon oxide (SiO_2) layers or ion-beam-synthesised silicon carbide (SiC) layers were grown on Si substrates. Implantation of silver (Ag), cobalt (Co) or tungsten (W) ions was performed sequentially on these dielectric layers to create Ag-SiO_2, Co-SiO_2 and WC-SiC nanocomposites.

We use the SiO_2 as the insulating host matrix because of its excellent chemical and physical stabilities, the simple and efficient fabrication process (thermal oxidation), and the well characterised and fast etching process (HF etching). Ag and Co are chosen for the metallic nanoclusters because they do not react chemically with the SiO_2 matrix and they form nano-sized pure clusters in silica [9,10]. On the other hand, SiC is a promising wide band-gap semiconductor material, with a number of attractive properties such as high electron mobility, high thermal conductivity, and excellent physical and chemical stabilities [11]. W implantation was preformed in SiC layer because W is a carbide-forming element and tungsten carbide (WC) is known to exhibit n-type metallic conduction, with an electrical resistivity lower than 17 μΩ·cm [12] and a work function of 3.6 eV [13]. Moreover, WC is also thermally, physically and chemically stable.

2. SAMPLE PREPARATION AND EXPERIMENTS

The substrates used in this work are n-type (100) Si wafers, with resistivity less than 0.05 Ω·cm. SiO_2 layers were thermally growth on the substrate by dry oxidation at 1000 °C. The thicknesses of the SiO_2 layers for the Ag and Co ion implantation were 120 and 150 nm, respectively. The Ag and Co ion implantations were preformed using a conventional high-current implanter, to a fixed dose of $5 \cdot 10^{16}$ ions/cm^2. The implantation energy was 110 keV for Ag^+ and was 50 keV for Co^+. The projected range of 110 keV Ag^+ ions and 50 keV Co^+ is found by SRIM simulation to be 58 nm and 45 nm, respectively [14].

The SiC layers used for W implantation were synthesised by high dose carbon implantation to a dose of $0.8 \cdot 10^{18}$ cm^{-2} into Si wafers, using a metal-vapor-vacuum-arc (MEVVA) ion source. The carbon plasma in MEVVA ion sources contains almost exclusively singly charged ions [15]. The details of the fabrication of the ion-beam-synthesised SiC layers were reported elsewhere [7]. Resulting layers were subsequently implanted with W ions at 70 kV using a fixed dose of $1 \cdot 10^{17}$ ions/cm^2. The W plasma contains ions of charge states 1^+ to 6^+, with particle current fractions as reported in [15]. This results in W ions with an energy of up to 420 keV, leading to a SRIM predicted range distribution peak-

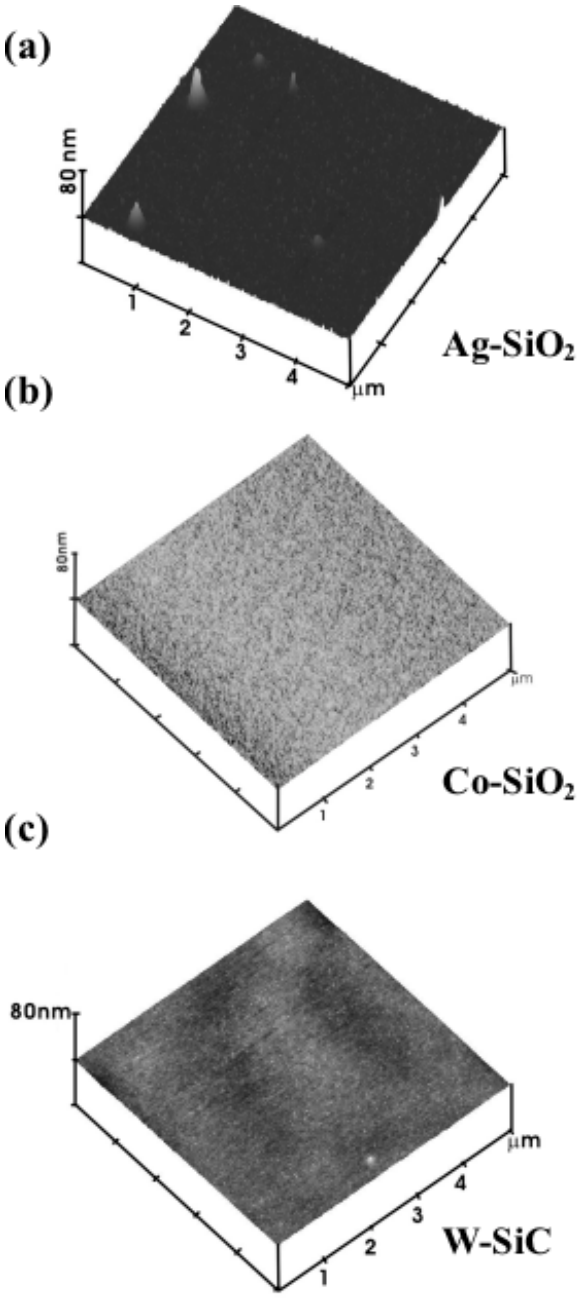

Fig. 1. AFM micrographs showing the surface morphology of the samples with implantation of (a) Ag ions on SiO_2 layer, (b) Co ions on SiO_2 layer and (c) W ions on SiC layer. The *x*- and *y*- scales are 1 μm/div and the *z*-scale is 40 nm/div in all the three micrographs.

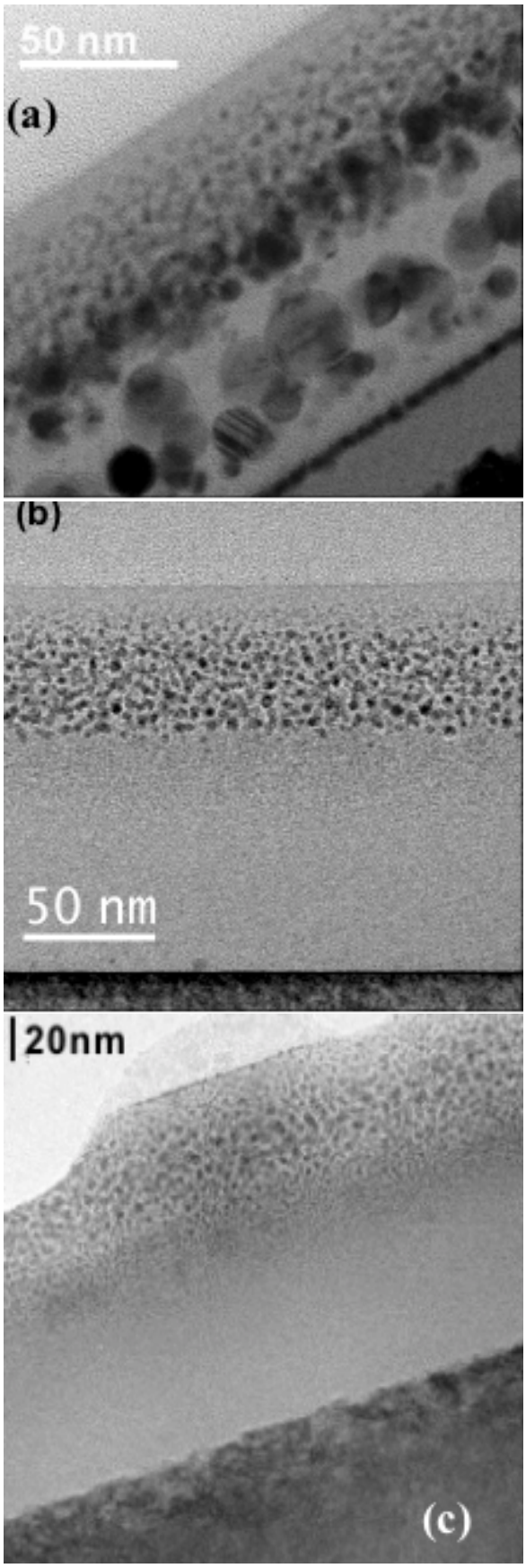

Fig. 2. Bright-field XTEM micrographs of the samples with implantation of (a) Ag ions on SiO_2 layer, (b) Co ions on SiO_2 layer, and (c) W ions on SiC layer.

ing at 60 nm and with a lower wing extending down to 180 nm.

The implantation doses were confirmed by Rutherford backscattering spectrometry (RBS) measurements, with a 1.56 MeV $^4He^+$ beam. The surface morphology was studied using atomic force microscopy (AFM). The microstructure was characterised using transmission electron microscopy (TEM). The chemical bonding conditions of the implanted tungsten ions were studied by X-ray photoelectron spectroscopy (XPS) with MoK_α source and 2 keV Ar sputtering for depth profiling. The FE properties of the Ag-SiO_2 and Co-SiO_2 samples were measured using a "sphere-to-plane" electrode configuration, with a 5 mm diameter stainless-steel ball anode in a high vacuum chamber ($\leq 5 \cdot 10^{-4}$ Pa) [16]. The anode was mounted on a Vacuum Generator HPT translator, which allowed FE maps to be carried out without the need for the sample to be returned to atmosphere. The applied electric field was obtained by dividing the applied voltage by the gap distance (typically, 50 μm). Alternatively, the FE properties of the W-SiC samples were measured using a 'parallel plane' electrode configuration, with a copper plate as the anode, in an ultra-high vacuum chamber ($\leq 3 \cdot 10^{-6}$ Pa) [7]. The separation between the sample surface and the Cu anode was 25 μm, maintained using a mica spacer, and the emission area was about 0.3 cm^2. Hence, the current density field (J-E) characteristics of the samples could be obtained.

3. RESULTS AND DISCUSSION

3.1. Ag-SiO_2 and Co-SiO_2 nanocomposites

The surface of the Ag-SiO_2 and Co-SiO_2 nanocomposite layers is very smooth, as shown in AFM measurements (Fig. 1). The root-mean-square (rms) values of surface roughness were determined to be 1.1 and 0.5 nm for Ag-SiO_2 and Co-SiO_2 nanocomposite layers, respectively. Hence, these layers lack any surface protrusions to provide significant geometric local field enhancement. The microstructure of these layers was studied by TEM. The cross-sectional TEM (XTEM) micrographs are shown in Fig. 2, and the statistical distributions of the metallic cluster sizes determined from the XTEM measurements are shown in Fig. 3.

Both of the implanted Ag and Co ions exist as nanoclusters in the SiO_2 layers, and these nanoclusters are identified as crystalline metal

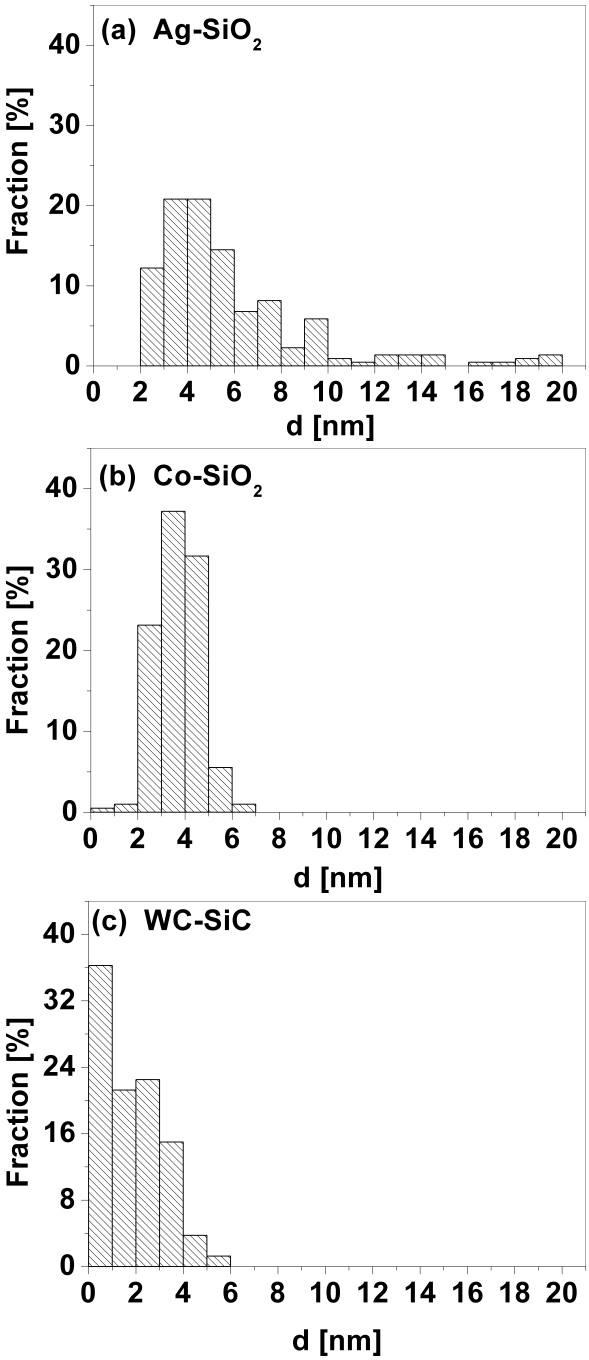

Fig. 3. The statistical distribution of metallic clusters within the samples with implantation of (a) Ag ions on SiO_2 layer, (b) Co ions on SiO_2 layer, and (C) W ions on SiC layer, as derived from XTEM.

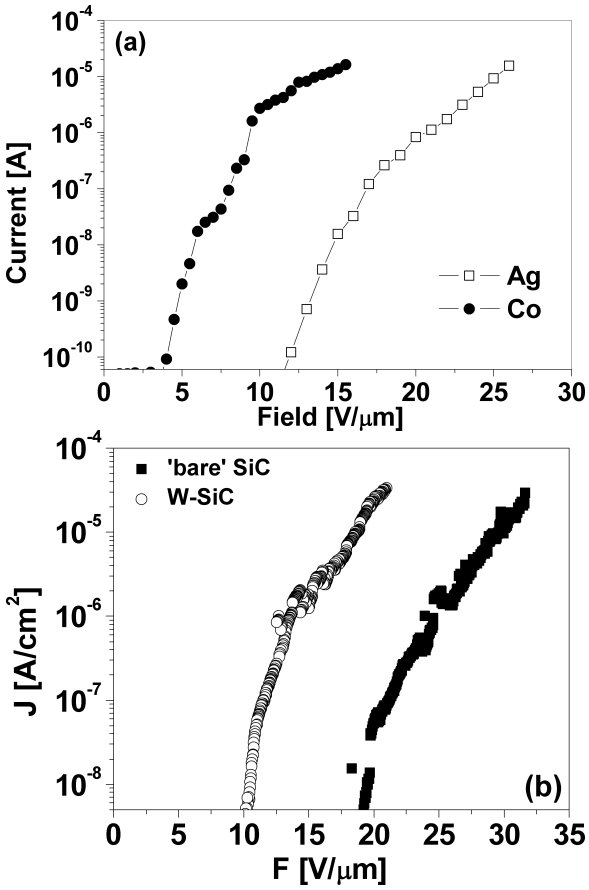

Fig. 4. The *I-F* characteristics of the samples with (a) Ag and Co implanted SiO_2 layers using "sphere-to-plane" electrode configuration and (b) W implanted SiC layer using "parallel plane" electrode configuration.

nanoparticles by high-resolution TEM and XPS measurements. However, the sizes and the distributions of the implanted metal clusters are very different in these two samples. As shown in Fig. 2 and Fig. 3, a relatively wide cluster size distribution is observed in the Ag implanted sample, with cluster sizes ranging from 2 to 20 nm in diameter. Near to the surface, the size of the Ag clusters is ~ 2-3 nm and these clusters act as emission sites for the FE process. As the depth from the surface is increased, the size and the concentration of the Ag clusters also increases. Ag clusters with sizes of ~ 9 nm, are located at a depth of 50 nm beneath the surface, which is close to the project range predicted by SRIM. Finally, Ag clusters with a maximum size of 20 nm are located at a depth of 80 nm beneath the surface. On the other hand, the Co implanted sample has a narrow cluster size distribution and the size of the clusters is much smaller

than that of the Ag-implanted sample, as shown in Fig. 2. The sizes of the Co nanoclusters are determined to be ~ 3.6 nm on average, and the maximum size of the Co nanoclusters is less than 7 nm, as compared with 20 nm of Ag nanoclusters. Besides, Co nanoclusters only appear at a depth up to ~ 100 nm beneath the surface, in contrast to the Ag implanted layer where Ag nanoclusters exist in the whole SiO_2 layer.

The 50 nm thick cobalt-deficient SiO_2 layer in the Co-implanted sample will prevent electrons transporting from the substrate to the vacuum during the electron FE process. Hence, in contrast to the conventional bottom electrical contact used in the Ag implanted sample in the FE measurement, a surface electrical contact was employed in the Co implanted sample. Thus electrons were allowed to flow through the conducting surface to emission sites and be emitted to the extraction electrode. It is noted that surface electrical contact was also employed in the Ag-implanted sample but it did not show any significant difference in the FE measurement results as compared to the conventional bottom contact method. The electron FE properties of these metal implanted SiO_2 layers are shown in Fig. 4. From the current-field (*I-F*) characteristics shown in Fig. 4a, the threshold fields (F_{th}), defined as the field strength where the emission currents reach 1 nA, are determined to be 13 and 5 V/μm for the Ag and Co implanted samples, respectively.

The *I-F* characteristics of 'bare' SiO_2 layers are also measured as control experiments (not shown) and the F_{th} is determined to be ~200 V/μm. Moreover, high-field conditioning took part in the FE process of the 'bare' SiO_2 layers, creating conductive paths for transporting the emissive electrons by dielectric breakdown, leading to surface destruction. However, the conditioning process is absent in the metal implanted layers because metallic nanoclusters within the SiO_2 layers can directly provide conductive paths for emissive electrons, hence, avoiding the surface destruction. Moreover, when an external field is present, the mobile charges in the layers will concentrate mainly at the boundaries of the localised metallic nanoclusters. Due to the nature of the electrical conductivity difference between the metallic nanoclusters and the SiO_2 matrix, the electric field lines will terminate at the mobile charge. This leads to a local electric field enhancement due to the electrical inhomogeneity [5-8], and hence, improves the F_{th} of the 'SiO_2' layers from ~200 V/μm to 12 and 5 V/μm after implantation of Ag and Co ions, respectively.

3.2. WC-SiC nanocomposites

At first, a uniform 160 nm thick amorphous SiC layer was achieved by carbon implantation. After tungsten implantation to a dose of $1 \cdot 10^{17}$ cm^{-2}, WC nanoclusters were formed with an average size of 2 nm, shown as dark dots in the XTEM micrograph shown in Fig. 2c. More than one third of the total clusters are less than 1 nm in size, which shown in Fig. 3. These dark dots were indeed WC confirmed by XPS measurements because the peak positions of the binding energies of W $4f_{7/2}$ electrons from various depths of the sample were determined to be ~32.0 eV. This value is nearer to the reported value of W $4f_{7/2}$ in WC (32.2 eV) compared with the reported values of W $4f_{7/2}$ in pure W (31.4 eV) [17] and WSi_2 (31.3 eV) [18]. The surface of the layer before and after W implantation is also atomically smooth (r.m.s < 0.5 nm), as shown in the AFM measurements (Fig. 1 and the AFM image of SiC layer is omitted). However, the turn-on field F_{on}, which is defined as the field strength where the emission current density reaches 1 μA/cm^2, decreased from 25 to 14 V/μm after W implantation (Fig. 4b). Therefore, it is evident that the metallic WC clusters do also lead to local field enhancement and provide conducting paths for the emissive electron in the SiC layer similar to the metal nanoclusters in the SiO_2 layers.

In comparison to SiO_2, SiC has excellent thermal conductivity, which is beneficial in the field emission devices in terms of stability. However, the SiO_2 has a more effective etching process (HF etching) which is useful for patterning the device structure.

4. CONCLUSION

In summary, the fabrication process of Ag-SiO_2, Co-SiO_2, and WC-SiC nanocomposites is reported. Their electron field emission properties are studied and are discussed in conjunction with their structural properties determined from measurements of AFM, TEM, and XPS. Results indicate clearly that metallic-dielectric nanocomposite layers have achieved excellent FE properties, with F_{th} as low as 5 V/μm. The good FE properties of these layers are attributed to the electrical inhomogeneity based local field enhancement due to embedded metallic nanoclusters.

ACKNOWLEDGEMENTS

One of us (W.M. Tsang) would like to acknowledge the financial support from the Croucher Founda-

tion. The financial support from the EPSRC in the form of a Portfolio Partnership Award is gratefully acknowledged. This work is also supported in part by the Germany - Hong Kong Joint Research Scheme sponsored by DAAD of Germany and RGC of Hong Kong SAR (Ref. No.: G_HK017/04).

REFERENCES

[1] P. Mazzoldi, G.W. Arnold, G. Battaglin, R. Bertoncello and F. Gonella // *Nucl. Instrum. Methods B* **91** (1994) 478 and references therein.
[2] P. D. Townsend // *Rep. Prog. Phys.* **50** (1987) 501.
[3] R.P. Cowburn // *J. Magn. Mater.* **242-245** (2002) 505.
[4] L. G. Jacobsohn, M. E. Hawley, D. W. Cooke, M. F. Hundley, J. D. Thompson, R. K. Schulze and M. Nastasi // *J. Appl. Phys.* **96** (2004) 4444.
[5] J.D. Carey, R.D. Forrest, R.U.A. Khan and S.R.P. Silva // *Appl. Phys. Lett.* **77** (2000) 2006.
[6] A. Ilie, A.C. Ferrari, T. Yagi and J. Robertson // *Appl. Phys. Lett.* **76** (2000) 2627.
[7] W.M. Tsang, S.P. Wong and J.K.N. Lindner // *Appl. Phys. Lett.* **81** (2002) 3942.
[8] N.S. Xu and S.E. Huq // *Mater. Sci. & Eng. R* **27** (2005) 47.
[9] G. Battaglin // *Nucl. Instr. and Meth. B* **116** (1996) 102.
[10] E. Cattaruzza // *Nucl. Instr. and Meth. B* **169** (2000) 141.
[11] Gary L. Harris, *EMIS datareviews series, No. 13, Properties of silicon carbide* (INSPEC publication, London, 1995).
[12] K. Bachmann and W.S. Williams // *J. Appl. Phys.* **42** (1971) 4406.
[13] *Carbide, Nitride and Boride Material – Synthesis and Processing*, ed. by A. W. Weimer (Chapman & Hall, London, 1997).
[14] J.F. Ziegler, J.P. Biersack and U. Littmark, *The stopping and range of ions in matter Vol.1* (Pergamon Press, New York 1985), www.srim.org.
[15] A. Anders // *Phys. Rev. E* **55** (1997) 969.
[16] R. D. Forrest, A. P. Burden, S. R. P. Silva, L. K. Cheah and X. Shi // *Appl. Phys. Lett.* **73** (1998) 3784.
[17] J. Luthin and Ch. Linsmeier // *Surface Science* **454-456** (2000) 78.
[18] G.S. Oehrlein and J.L. Lindstom // *J. Vac. Sci. Technol. A* **7** (1989) 1035.